PNAS Nexus, 2023, 2, 1–15
https://doi.org/10.1093/pnasnexus/pgad135
Advance access publication 13 April 2023
Research Report

Cis mutagenesis in vivo reveals extensive noncanonical functions of Dscam1 isoforms in neuronal wiring

Shixin Zhang[a,1], Xi Yang[b,1], Haiyang Dong[a], Bingbing Xu[a], Lili Wu[a], Jian Zhang[a], Guo Li[a], Pengjuan Guo[a], Lei Li[a], Ying Fu[a], Yiwen Du[a], Yanda Zhu[a], Jilong Shi[a], Feng Shi[a], Jianhua Huang[c], Haihuai He[d,*] and Yongfeng Jin[a,*]

[a]MOE Laboratory of Biosystems Homeostasis & Protection and Innovation Center for Cell Signaling Network, College of Life Sciences, Zhejiang University, Hangzhou ZJ310058, People's Republic of China
[b]Cancer Center and State Key Laboratory of Biotherapy, West China Hospital, Sichuan University, Chengdu 610041, People's Republic of China
[c]Institute of Insect Sciences, Zhejiang University, Hangzhou ZJ310058, People's Republic of China
[d]Department of Neurosurgery, Cancer Center and State Key Laboratory of Biotherapy, West China Hospital, Sichuan University, Chengdu 610041, People's Republic of China
*To whom correspondence should be addressed: Email: haihuai.he@scu.edu.cn (H.H.); jinyf@zju.edu.cn (Y.J.)
[1]S.Z. and X.Y. contributed equally to this work.
Edited By: Nancy Bonini

Abstract

Drosophila Down syndrome cell adhesion molecule 1 (*Dscam1*) encodes tens of thousands of cell recognition molecules via alternative splicing, which are required for neural function. A canonical self-avoidance model seems to provide a central mechanistic basis for Dscam1 functions in neuronal wiring. Here, we reveal extensive noncanonical functions of Dscam1 isoforms in neuronal wiring. We generated a series of allelic *cis* mutations in *Dscam1*, encoding a normal number of isoforms, but with an altered isoform composition. Despite normal dendritic self-avoidance and self-/nonself-discrimination in dendritic arborization (da) neurons, which is consistent with the canonical self-avoidance model, these mutants exhibited strikingly distinct spectra of phenotypic defects in the three types of neurons: up to ~60% defects in mushroom bodies, a significant increase in branching and growth in da neurons, and mild axonal branching defects in mechanosensory neurons. Remarkably, the altered isoform composition resulted in increased dendrite growth yet inhibited axon growth. Moreover, reducing Dscam1 dosage exacerbated axonal defects in mushroom bodies and mechanosensory neurons but reverted dendritic branching and growth defects in da neurons. This splicing-tuned regulation strategy suggests that axon and dendrite growth in diverse neurons cell-autonomously require Dscam1 isoform composition. These findings provide important insights into the functions of Dscam1 isoforms in neuronal wiring.

Keywords: Dscam1 diversity, isoform composition, noncanonical function, self-avoidance, neuronal wiring

Significance Statement

Complex animals require distinct cell surface recognition molecules to specify the assembly of neural circuits. In fly, *Dscam1* encodes 38,016 isoforms via alternative splicing. A canonical model is that Dscam1 diversity provides neurons with a unique code for self-avoidance and self-/nonself-discrimination. However, the prevalence of this self-avoidance providing a mechanistic basis for Dscam1 functions remains unclear. Here, we explore a splicing-tuned strategy to reveal additional phenotypes that cannot be easily explained by alterations in self-avoidance, demonstrating the extensive noncanonical function of Dscam1 isoforms. These data suggest that Dscam1 isoform composition is cell-autonomously required for at least some developmental contexts. Our finding expands the current understanding of the function of Dscam1 diversity in neural circuit formation, in addition to mediating self-avoidance.

Introduction

Developing neurons interact in specific and stereotyped ways to form neural circuits that underlie complex nervous functions. Over the past two decades, several large gene families associated with cell surface recognition have been identified, including the fly *Down syndrome cell adhesion molecule 1* (*Dscam1*) and the vertebrate-clustered *Pcdhs* (1, 2). *Drosophila Dscam1* encodes 38,016 isoforms through alternative splicing of four exon clusters in exons 4, 6, 9, and 17, each containing one of 19,008 alternative ectodomains linked to one of the two alternative transmembrane domains (1) (Fig. S1A). Identical Dscam1 ectodomains interact strongly and mediate homophilic repulsion, but the interactions between different ectodomains are weak (3). Each neuron expresses only a small subset of Dscam1 isoforms (10–50 isoforms) in a biased but stochastic manner, conferring a unique molecular identity to each individual neuron for self-recognition in the

Competing Interest: The authors declare no competing conflict of interest.
Received: February 14, 2023. **Revised:** April 4, 2023. **Accepted:** April 6, 2023

nervous system (4–6). This splicing pattern combined with strict homophilic binding specificity leads to repulsion between the neurites of a single neuron, while allowing contact with other neurons of the same type. Genetic studies have shown that thousands of isoforms are required to distinguish self from nonself during self-avoidance as well as the normal patterning of axons and dendrites (7, 8). In this scenario, no specific isoforms are required; what is important is that a neuron expresses a subset of isoforms that are different from other neurons (6–13).

Although the canonical self-avoidance mechanism has been elegantly illustrated in the dendrite spacing of fly larval PNS neurons and the axonal branching bifurcation of mushroom body (MB) neurons, whether this model alone can explain all the mechanistic bases for Dscam1 isoform functions in neural circuit assembly remains inadequately addressed. Previous work reported that cell-autonomous reduction of Dscam1 isoform diversity to potential 396 isoforms in a single adult mechanosensory (MS) neuron causes impairment of growth cone sprouting, which leads to severe disruption of collateral formation (10). It appears that the ratio of matching and nonmatching isoforms within a neuron determines the Dscam1-mediated signaling strength, which in turn regulates axonal branch formation. Moreover, Kim et al. (13) observed that expression of only a single Dscam1 isoform variant by using intragenic MARCM in a single larval sensory neuron resulted in a reduction in presynaptic arbor size. Apparently, in these contexts, Dscam1 isoform diversity plays a noncanonical role in axon branching and growth. In addition, the RNAi knockdown of Dscam1 in embryonic motor neurons has been shown to cause only defective dendrite growth and branching, with dendrite spacing is not affected (14). Recently, RNAi knockdown of Dscam1 revealed diverse neuron-type-specific roles during central neuron arbor differentiation (15). These studies suggest that, at least in some neurons, self-avoidance alone is insufficient to provide all the mechanistic bases for Dscam1 functions.

Indeed, these functional experiments using RNAi knockdown, knock-in, or genomic deletion either result in changes in overall protein levels, reduced isoform diversity, or both (1, 6, 9, 14, 16–25). Therefore, it remains unclear whether these defective phenotypes observed in mutants are caused by changes in Dscam1 protein levels, isoform numbers, or both. Importantly, the phenotypic defects resulting from reduced isoform diversity may be due not only to loss of function but also to gain of function associated with increased expression of the remaining isoforms (10, 26). Moreover, the reduction in isoform diversity leads to a dispute: ectopic interactions, as it is difficult to distinguish whether these neuronal developmental defects are due to the reduced diversity of the cells themselves or to interactions between cells with both reduced diversity. A definitive strategy to address the noncanonical functions of Dscam1 diversity is to construct mutant flies that express identical protein levels to wild-type (WT) controls but with a comparable number of isoforms. These mutants are sufficient to confer normal self-avoidance and self-/nonself-discrimination. We envision that if these mutant flies exhibit significant phenotypic defects, then such defects should be attributed to the noncanonical role of Dscam1 isoforms rather than to self-avoidance. Recently, we deleted downstream docking sites of *Dscam1* exon 4 or 9 clusters to construct splicing bias-altering mutants that exhibit subtle to mild MB axonal defects (27). Generation of additional mutants by changing noncoding *cis*-elements will allow exploration of the noncanonical role of Dscam1 isoforms.

In this study, we used in vivo *cis* mutagenesis to construct mutant flies that encode a comparable number of Dscam1 isoforms as WT but with an altered isoform composition. These mutants exhibit normal dendritic self-avoidance and self-/nonself-discrimination in dendritic arborization (da) neurons, which is consistent with the canonical self-avoidance model. Surprisingly, these mutants exhibit strikingly distinct spectra of phenotypic defects in three types of neurons: up to ~60% defects in mushroom bodies, a significant increased branching and growth in da neurons, and mild axonal branching defects in MS neurons. Moreover, removal of one copy of the mutant *Dscam1* exacerbates defects in mushroom bodies and MS neurons but reverts the dendritic branching and growth of da neurons. Considering the highly biased expression of exon 9s in various neurons, the composition of Dscam1 Ig7 variants may be of general importance in regulating neuronal wiring. These data suggest that Dscam1 isoform composition is cell-autonomously required for normal growth in diverse neurons.

Results

Construction of mutant flies with normal Dscam1 overall protein levels and an identical isoform number but with an altered Ig7 composition

The initial aim of this study was to explore the molecular mechanism underlying the alternative splicing of exon cluster 9 encoding the Ig7 domain in *Drosophila Dscam1*. We have previously identified the docking site in the intron upstream of *Drosophila Dscam1* exon 10, which may pair with the selector sequence downstream of only a few exon 9 variants (27, 28). Considering the presence of dual docking sites and bidirectional base pairings in the exon 9 cluster of distantly related lepidopteran, coleopteran, and hymenopteran *Dscam1* (Fig. 1A) (29, 30), we speculate that an analogous docking site may be located in the intron upstream of exon 9.1 of *Drosophila Dscam1*. However, sequence alignment revealed only relatively limited conservation across *Drosophila* species (Fig. S1B). Since these introns are only ~150 nt in size, we speculate that an analogous upstream docking site, if present, would be located in the middle region of intron 8. To address this issue, we used CRISPR/Cas9 technology to delete the middle intronic region and then investigated the effect on exon 9 inclusion variants. We generated a series of homozygous viable flies with varying degrees of deletion (designated as $Dscam1^{\Delta 9uD1-\Delta 9uD5}$) (Fig. 1A). We did not observe obvious phenotypic defects in all $Dscam1^{\Delta 9uD1-\Delta 9uD5}$ adults. Reverse transcription PCR (RT-PCR) analysis showed no significant differences in the overall inclusion of exon 9 in the head of $Dscam1^{\Delta 9uD}$ compared with WT as well as at different developmental stages (Fig. 1B). Western blot analysis revealed that the Dscam1 level was indistinguishable between $Dscam1^{\Delta 9uD}$ and the WT (Fig. 1C). These data indicate that $Dscam1^{\Delta 9uD}$ mutant flies display normal Dscam1 expression levels as WT controls.

To determine how the expression of individual exon 9 variants changes in $Dscam1^{\Delta 9uD}$ mutants, we examined the relative use of exon 9 variants in RT-PCR products containing exon 9 using high-throughput sequencing. Sequencing analysis revealed a change in the frequency of exon 9 variants in $Dscam1^{\Delta 9uD}$ flies (Fig. 1D). The $Dscam1^{\Delta 9uD1}$ mutant with the smallest deletion exhibited subtle changes in exon 9s frequency, while the $Dscam1^{\Delta 9uD2-\Delta 9uD5}$ with the larger deletion exhibited global changes in exon 9 inclusion. Interestingly, we found that the inclusion frequencies of most exon 9s were decreased except for exons 9.1 and 9.

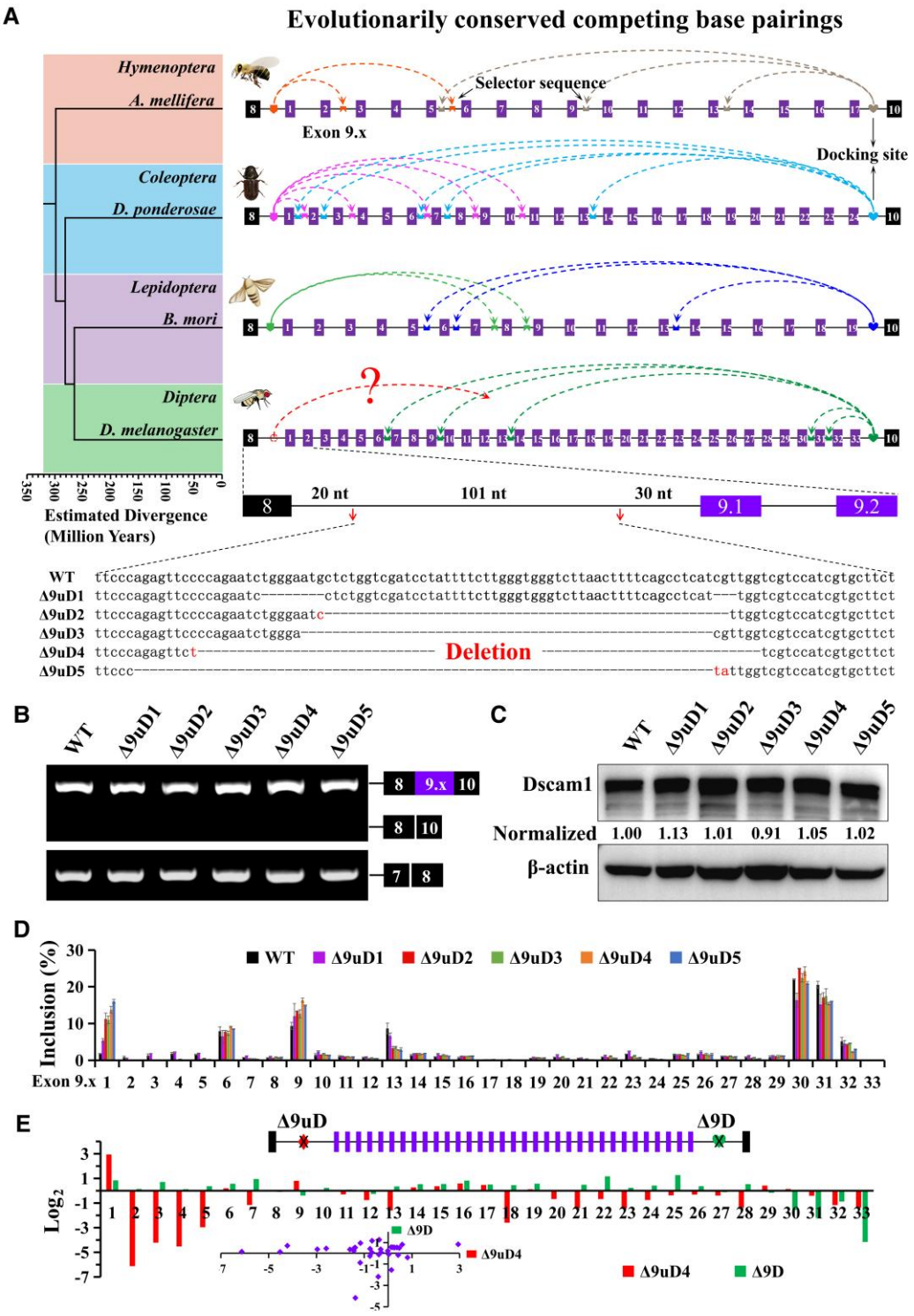

Fig. 1. Construction and characterization of Dscam1 isoform composition-altered mutants (see also Fig. S1). A) A phylogeny of conserved base pairings in governing alternative splicing of exon 9 clusters during insect evolution. Exons, docking sites, and selectors are not drawn to scale. Sequence-specific docking sites and selector sequences are shown in different colors. The dashed arrow represents the base pairing interaction between the docking site and selector sequence. Interintronic base pairings in *Drosophila melanogaster* were confirmed (27). Base pairings between the docking site and the selector sequence for the exon 9 cluster of lepidopteran *Dscam1* were experimentally verified (29). Base pairings between the docking site and the selector sequence in the hymenopteran *Apis mellifera* and the coleopteran *Dendroctonus ponderosae* were predicted by comparative genome comparison and structural modeling (29, 30). These competing base pairings are conserved, but the docking site and selector sequence are clade specific. Considering the presence of dual docking sites and bidirectional base pairings in the lepidopteran, coleopteran, and hymenopteran *Dscam1*, we speculate that an analogous docking site may be located in the *Drosophila Dscam1* (shown by the dashed line plus "?"). The arrow in intron 8 indicates the position of the designed sgRNAs. The dashed lines represent the deleted sequences. B) RT-PCR analysis showing that the overall inclusion of exon 9 is not affected. C) Western blot analysis showing that the Dscam1 level of *Dscam1*$^{\Delta 9uD}$ was indistinguishable from that of the WT control. D) *Dscam1*$^{\Delta 9uD}$ mutants showing a mild to global alteration in the expression of a single exon 9 variant compared to the WT control. E) The $\log_2$ fold change in the frequency of variable exon 9 inclusion in *Dscam1*$^{\Delta 9uD4}$ largely contrasting with the change pattern in *Dscam1*$^{\Delta 9D}$, which lacks the downstream docking site (27). Data are expressed as mean ± SD.

Remarkably, exon 9.1 inclusion increased 8-fold, from 2% in WT to 16% in *Dscam1*$^{\Delta 9uD5}$ mutants having the largest deletion (Fig. 1D). In addition, we observed a shared and specific change in expression at different developmental stages of mutant flies (Fig. S1C–F). Notably, except for a few exon 9s, this pattern of frequency changes in most exon 9 variants of *Dscam1*$^{\Delta 9uD4}$ mutants largely contrasts with the changing pattern of *Dscam1*$^{\Delta 9D}$ mutants, which lack the downstream docking site (Fig. 1E) (27). These data demonstrate the involvement of deleted sequences in determining the choice of exon 9 variants.

Altered isoform expression at a single-neuron resolution

We next sought to determine the altered expression spectra of Dscam1 isoforms at a single-neuron resolution. Detection of the Dscam1 isoform pool in single cells is technically challenging due to the low expression of Dscam1 in the nervous system and the low sensitivity of the two-round RT-PCR strategy adopted in prior studies (4, 6, 10). To explore this issue, we performed single-cell analysis of class I da and MB neurons by fluorescence-activated cell sorting using SMART-seq2 (31). Class I da neurons were specifically labeled with *221-GFP Gal4* to drive UAS-mCD8-GFP expression, and the whole MB was labeled with OK107-Gal4. As expected, individual class I da neurons expressed multiple exon 9 variants in a stochastic but biased manner (Fig. 2A). Compared with WT and *Dscam1*$^{\Delta 9uD1}$, exon 9.1, exons 13–16, and exons 20–24 exhibited increased expression in individual single cells of *Dscam1*$^{\Delta 9uD2–\Delta 9uD5}$ (Fig. 2A). Surprisingly, MB neurons express a much broader spectrum of multiple exon 9 variants at a single-neuron resolution compared with class I da neurons (Fig. 2B). We observed that each MB neuron expresses up to 15–22 exon 9 variants, which is much higher than the 3–5 exon 9 variants per neuron in previous studies (6). In this context, if variable exon 4s and exon 6s are combined, each MB neuron may express up to hundreds of Dscam1 isoforms. Similarly, each MB neuron in *Dscam1*$^{\Delta 9uD2–\Delta 9uD5}$ expresses a comparable number of exon 9 variants to WT. However, considerable variation in expression patterns was observed in individual MB neurons between WT and mutants. Remarkably, exon 9.1 inclusion was remarkably increased in *Dscam1*$^{\Delta 9uD2–\Delta 9uD5}$ single neurons (Fig. 2B). Overall, the isoform diversity of our generated mutant flies is largely unchanged compared to WT, but the composition of exon 9 encoding the Ig7 domain is altered in each neuron type (Fig. 2C). These viable homozygous mutants allowed us to explore the role of Dscam1 isoform composition in fly development and neuronal wiring. Next, we focused on assessing the phenotypic defects of the three types of neurons in *Dscam1*$^{\Delta 9uD1–\Delta 9uD5}$ mutants.

Altered composition of Ig7 variants causes subtle to mild fly viability and locomotion defects

We next investigated the effect of deletion on the survival of *Dscam1*$^{\Delta 9uD1–\Delta 9uD5}$ mutant flies from embryonic to adult stages. The survival rates of *Dscam1*$^{\Delta 9uD1–\Delta 9uD5}$ embryos decreased mildly as the deletion size increased (Fig. 2D). *Dscam1*$^{\Delta 9uD1}$ mutants exhibited a subtle survival defect, but *Dscam1*$^{\Delta 9uD4}$ and *Dscam1*$^{\Delta 9uD5}$ mutants exhibited a survival rate of ~75% compared with 92% for the WT control (Fig. 2D). The difference in survival rate was mainly reflected in the embryo hatching stage, while no significant difference was observed in pupation and eclosion rates. These data suggest that the altered Ig7 isoform composition is detrimental to embryonic development.

To investigate the effect of altered Ig7 isoform composition on fly behavior, we analyzed the crawling ability of *Dscam1*$^{\Delta 9uD1–\Delta 9uD5}$ mutant larvae. We observed a subtle to mild decrease in the crawling ability of mutant larvae with increasing deletion size (Fig. 2E, panel i). Furthermore, the locomotion ability of *Dscam1*$^{\Delta 9uD1–\Delta 9uD4}$ was not significantly different from that of WT adults, except for *Dscam1*$^{\Delta 9uD5}$, which had the largest deletion (Fig. 2E, panel ii). Taken together, these data indicate that the proper composition of Dscam1 Ig7 variants is required for normal fly viability and locomotion.

Dscam1$^{\Delta 9uD}$ exhibits normal dendritic self-/nonself-discrimination but an obvious increased branching and growth of da neurons

To examine the potential role of Dscam1 diversity in dendritic wiring, we compared dendritic morphology between *Dscam1*$^{\Delta 9uD}$ mutants and WT in da neurons. There were no significant differences in the characteristic overall shape or dendritic territory borders of *Dscam1*$^{\Delta 9uD}$ mutants compared with controls (Fig. 3A). As expected, the self-dendrites of class I da neurons in *Dscam1*$^{\Delta 9uD1–\Delta 9uD5}$ mutants avoid each other as in WT controls, whereas *Dscam1*^{null} mutants exhibit severe overlap and fasciculation of the self-dendrites (Fig. 3A and B). In addition, similar dendritic self-repulsion was observed in two other types of class I neurons (ddaD and ddaE) of *Dscam1*$^{\Delta 9uD2–\Delta 9uD5}$ mutants (Figs. S2B, C, and F and S3A). Furthermore, we found no significant difference in the number of overlaps between class I (vpda) and class III (v′pda) dendrites compared with various *Dscam1*$^{\Delta 9uD1–\Delta 9uD5}$ mutants and WT controls (Figs. 3C and S3B). These results from phenotypic analysis are consistent with the single-neuron data in *Dscam1*$^{\Delta 9uD1–\Delta 9uD5}$ mutants (Fig. 2A), which is compatible with a role of Dscam1 isoforms in neural self-avoidance and self-/nonself-discrimination.

We next compared the dendritic length and branch number between *Dscam1*$^{\Delta 9uD}$ mutants and the WT control. Quantification revealed that the total dendritic length of *Dscam1*$^{\Delta 9uD2–\Delta 9uD5}$ mutants was significantly greater than that of WT neurons, while *Dscam1*$^{\Delta 9uD1}$ mutants exhibited a slight increase (Fig. 3D). The total dendritic branch number of *Dscam1*$^{\Delta 9uD2–\Delta 9uD5}$ mutants was significantly increased by 40–80% (Fig. 3E). In particular, in *Dscam1*$^{\Delta 9uD2}$ mutants, the total number of dendritic branches per neuron increased to 70, accounting for almost twice the number of 37 in WT controls. Further analysis revealed that these increases were caused by additional tertiary and quaternary branches, but primary and secondary dendrites were not greatly affected (Fig. 3F), indicating that Dscam1 is involved in the formation of dendritic branches. Since *Dscam1*$^{\Delta 9uD}$ alleles express overall similar expression levels and generate a comparable number of Dscam1 isoforms as WT controls, we conclude that these increased branches should be attributed to the altered composition of Dscam1 Ig7 variants. These data also suggest that Dscam1 isoforms are intrinsically required for normal dendrite growth and branching of class I neurons.

Similarly, we observed a notable increase in the total dendritic length of ddaD and ddaE neurons in *Dscam1*$^{\Delta 9uD2–\Delta 9uD5}$ mutants compared with WT (Fig. S2D and G). *Dscam1*$^{\Delta 9uD2–\Delta 9uD5}$ mutants exhibited significant increases in the total number of dendritic branches in ddaD and ddaE neurons (Fig. S2E and H). Notably, there were considerable differences in the length and number of dendrite branches among the different *Dscam1*$^{\Delta 9uD}$ mutants (Figs. 3 and S2), suggesting that the specific Dscam1 repertoire of each cell may play an intricate role in dendrite

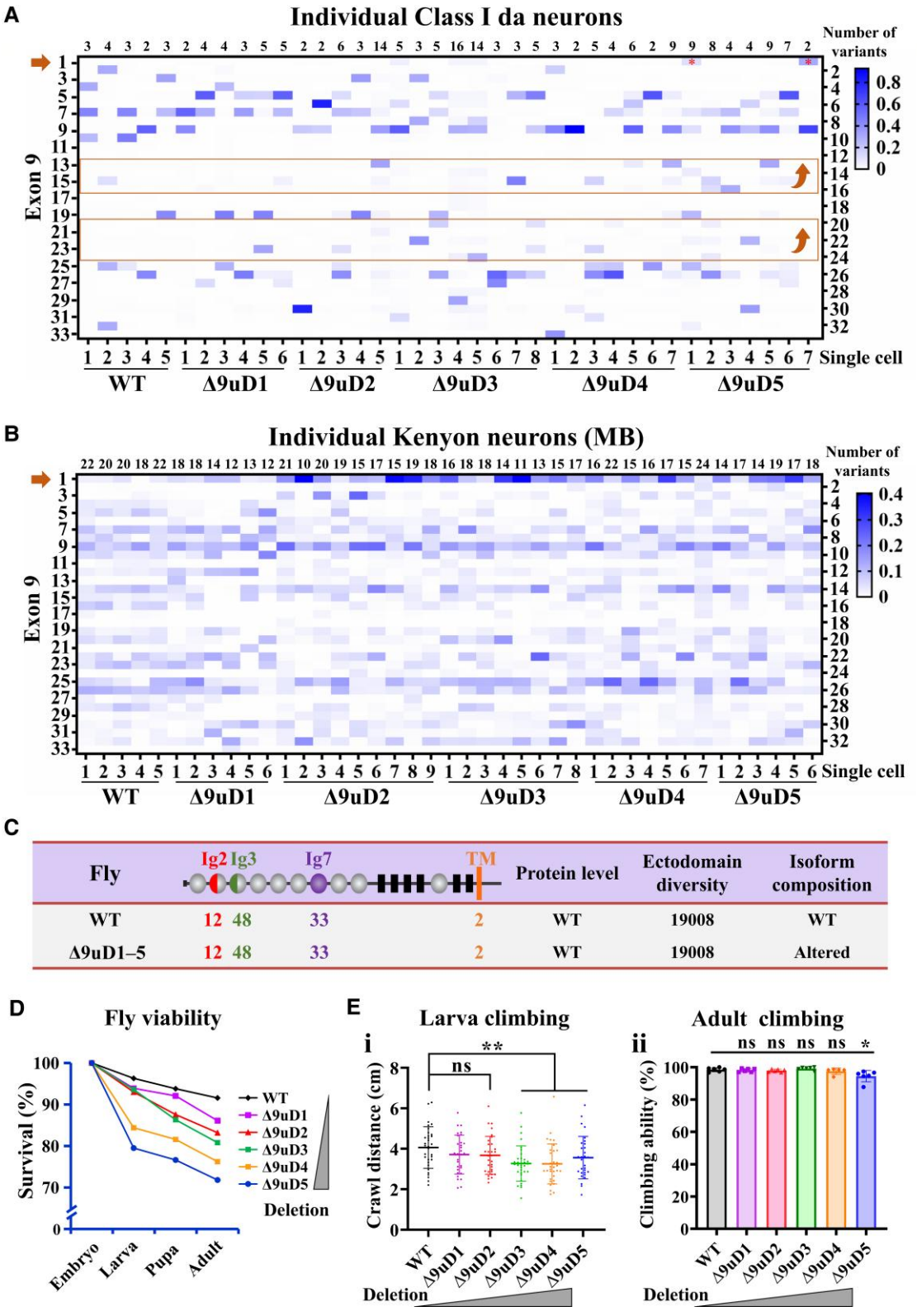

Fig. 2. Exon 9 expression pattern of individual class I da neurons and MB neurons. A) Individual class I da neurons expressing multiple exon 9 variants in a stochastic but biased manner. The inclusion of exon 9.1 with increased expression is marked with a brown arrow and other exons with increased expression are indicated by brown frames. The number of exon 9 variants expressed in each cell (>0.01 threshold) is indicated at the top of the heat map. B) Individual Kenyon cells expressing a broader spectrum of multiple exon 9s in the *Dscam1*$^{\Delta 9uD2-\Delta 9uD5}$. The inclusion of exon 9.1 with increased expression is marked with a brown arrow. C) Characterization of *Dscam1*$^{\Delta 9uD}$ compared with WT. D) Survival rates of WT and *Dscam1*$^{\Delta 9uD}$ mutants during development. E) Effect of altered expression of exon 9 variants on fly locomotion. The climbing ability of mutant larva (i) and adult (ii) was tested. Data are expressed as mean ± SD. ns, not significant; *, $P < 0.05$; **, $P < 0.01$ (Student's *t*-test, two-tailed).

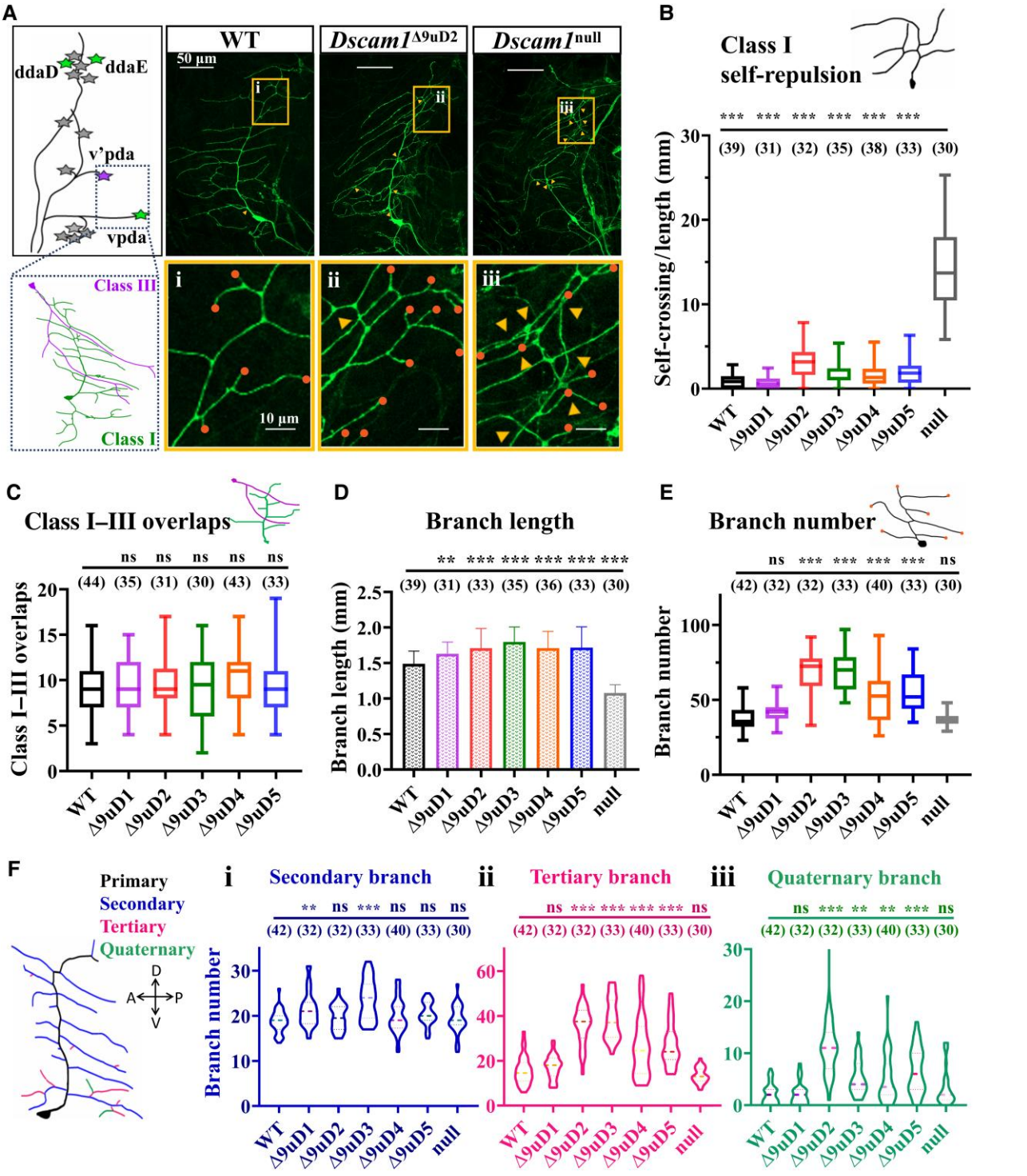

Fig. 3. *Dscam1*$^{\Delta 9uD2-\Delta 9uD5}$ mutants showing an increased branching in class I da neurons (see also Figs. S2 and S3). A) Schematic representation of an abdominal hemisegment of da neurons. Representative images of da neuron dendrites in different *Dscam1* mutants are shown. Scale bars, 50 μm. Boxes in images indicate detailed views in i, ii, and iii to illustrate that *Dscam1*$^{\Delta 9uD2-\Delta 9uD5}$ show a slight increase in self-crossing compared to *Dscam1*^{null} and a marked increase in the number of branches. Scale bars, 10 μm. Arrowheads indicate points of self-crossing between sister branches, and dots represent branches in the selected area. B) *Dscam1*$^{\Delta 9uD}$ vpda showing significant differences in self-crossing compared to *Dscam1*^{null}. C) The numbers of overlaps between class I and class III dendrites are indistinguishable between *Dscam1*$^{\Delta 9uD1-\Delta 9uD5}$ mutants and WT controls. D) Total dendritic length of *Dscam1*$^{\Delta 9uD2-\Delta 9uD5}$ being longer than that of WT neurons. E) Vpda showing a significant increase in total branches in *Dscam1*$^{\Delta 9uD2-\Delta 9uD5}$. F) Vpda showing an increase in branches in *Dscam1*$^{\Delta 9uD2-\Delta 9uD5}$. Vpda is divided into four branches, with reference to previous studies (46). The primary branch is the limb (color in black), the secondary branch grows directly from the middle primary branch (color in blue), the tertiary branch is the small side branch on the secondary branch (color in pink), and the quaternary branch is another smaller branch (color in green). The tertiary branches and quaternary branches are increased observably in *Dscam1*$^{\Delta 9uD2-\Delta 9uD5}$. Numbers in parenthesis are neurons analyzed. Data in the boxplot are represented as median (dark line), 25–75% quantiles (box), and error bars (1.5 × quartile range). *, $P < 0.05$; **, $P < 0.01$; ***, $P < 0.001$; ns, not significant (Student's *t*-test, two-tailed).

formation. Taken together, our results indicate that Dscam1 isoforms are required not only to discriminate between self and nonself neurites but also for normal dendrite growth and branching in *Drosophila* da neurons. The former role does not require specificity but rather the number of isoforms, whereas the latter role involves the specificity of isoforms, at least for Ig7 variants.

Dscam1$^{\Delta 9uD4}$ and *Dscam1*$^{\Delta 9uD5}$ exhibit >50% MB defects

Next, we evaluated whether and how the altered composition of Ig7 variants leads to morphological defects in the mushroom bodies of the adult fly brain. The MB consists of ~2,500 neurons, most of which have two branches projecting to two orthogonal paths, forming a bilobed structure (32). It has been shown that expression of a single Dscam1 isoform is sufficient to support self-branches with high-fidelity segregation and that thousands of isoforms are required to ensure normal MB lobe segregation (8); unexpectedly, we observed 17–67% MB morphological defects in *Dscam1*$^{\Delta 9uD2–\Delta 9uD5}$ mutant flies. The defective morphologies included absence, truncation, thinning, and misprojection of lobes (Fig. 4). The largest phenotypic defects in these mutants were one lobe absent and one lobe thinner. In addition, the MB phenotype improved as the deletion size decreased (Fig. 4B). In particular, we found that 67 and 56% of brain hemispheres displayed MB morphological defects in *Dscam1*$^{\Delta 9uD4}$ and *Dscam1*$^{\Delta 9uD5}$ mutant flies, respectively (Fig. 4B). Notably, such a high penetrance of MB defects contrasts starkly with the ~14% (not including the β-lobe fusion) of MB defects of *Dscam1*$^{\Delta 9D}$ mutants, which lack the downstream docking site (27). Moreover, the *trans*-heterozygous mutant *Dscam1*$^{\Delta 9uD4}$/*Dscam1*$^{\Delta 9uD5}$ showed abnormal MB phenotypes in 50% of the brain hemispheres, closely similar to the *Dscam1*$^{\Delta 9uD4}$ and *Dscam1*$^{\Delta 9uD5}$ mutants (Fig. 4B). All *Dscam1*$^{\Delta 9uD2–\Delta 9uD5}$/*Dscam1*$^{+}$ heterozygous mutants exhibited <5% MB phenotypic defects (Fig. 4B).

To exclude the possibility of off-target effects leading to morphological defects, we independently constructed two homozygous mutants (designated as *Dscam1*$^{\Delta 9uD4*}$ and *Dscam1*$^{\Delta 9uD5*}$) using homologous recombination, which lack the same sequence as *Dscam1*$^{\Delta 9uD4}$ and *Dscam1*$^{\Delta 9uD5}$, respectively (Fig. S4). These *Dscam1*$^{\Delta 9uD4*}$ and *Dscam1*$^{\Delta 9uD5*}$ mutants exhibit a spectrum of phenotypic defects in MB that are comparable with the *Dscam1*$^{\Delta 9uD4}$ and *Dscam1*$^{\Delta 9uD5}$ mutants, respectively (Fig. 4B). Therefore, we conclude that such a high penetrance of the defective morphology in MB should be attributed to the overall altered composition of Dscam1 Ig7 variants. Since *Dscam1*$^{\Delta 9uD}$ alleles express Dscam1 at an overall similar level and encode a comparable number of Dscam1 isoforms as WT controls, the high penetrance of MB defective phenotypes cannot be fully explained by the canonical self-avoidance model (7, 8).

Altered composition of Ig7 variants causes extensive MB axonal growth and branching defects in single-cell clones

To further investigate the molecular mechanisms underlying the morphological defects of MB in *Dscam1*$^{\Delta 9uD}$ mutants, we used MARCM analysis to examine the axonal projections of MB neurons at single-cell resolution (32). Compared with WT control clones ($\underline{n} = 29$), more than 40% of *Dscam1*$^{\Delta 9uD}$ mutant neurons ($n > 30$) exhibited a growth defect (formation of shortened branches), or a branching defect, or a misguidance defect, or sometimes a combination of these (Fig. 5A and B). The overall penetrance of MB defects correlated strongly with defects revealed in single clones (Fig. 5C). Axon growth appears to be most sensitive to changes in Ig7 variants of Dscam1. Axonal growth defects exhibited mainly shortened branches, accounting for ~55% of all defects in *Dscam1*$^{\Delta 9uD2–\Delta 9uD5}$ (Fig. 5D). This axonal shortening is consistent with the presence of truncated lobes (Fig. 4B), suggesting that the presence of truncated lobes may be caused by impaired axon growth.

The axon branching was also sensitive to changes in Ig7 variants, accounting for ~40% of axonal defects (Fig. 5B). Branching defects include the generation of α- but not β-axonal branches without axon bifurcation at the peduncle end and vice versa (Fig. 5A). About 10–45% of single neurons exhibit such defects in *Dscam1*$^{\Delta 9uD2–\Delta 9uD5}$ (Fig. 5E). Single branches can explain the absence and thinning phenotypes in MB, even no lobe when growth defects and bifurcation defects occur simultaneously. Besides, other defects include misguidance and multibranching, which may cause a missing or misguided lobe and a thinner or thicker lobe. These observations indicate that the absence of a specific lobe, thinning, thickening, and misprojection of one lobe, as observed in whole brains of fly mutants (Fig. 4), is caused by a combination of failure in axon branching and misguidance. These data show that even repertoires expressing up to thousands of Dscam1 isoforms appear to be insufficient to achieve a normal axonal patterning. Taken together, these phenotypic studies indicate that the composition of Dscam1 Ig7 variants is critical for normal growth, branching, and guidance of MB axons.

We then examined how altered composition of Dscam1 isoforms affects self-avoidance of MB axonal branches. A fundamentally different role for Dscam1 isoform diversity in regulating branch segregation was proposed in a previous study in which axonal sister branch segregations in MB neurons were analyzed in different *Dscam1*^{single} mutants that express only a single ectodomain from an endogenous locus (7, 22). The latter found that the sister branches of isolated *Dscam1*^{single} MB neurons segregated with high fidelity. In contrast to previous work (7, 22), our data demonstrate that even expression of a repertoire of up to thousands of Dscam1 isoforms (encoded within the genome of a single cell) appears to be insufficient for normal sister branch segregation. We found that bifurcated sister branches often fail to separate correctly in *Dscam1*$^{\Delta 9uD2–\Delta 9uD5}$ mutants, such as in *Dscam1*^{null} (Fig. S5A and C). For example, up to 24% of *Dscam1*$^{\Delta 9uD4}$ axons with bifurcated sister branches failed to segregate reliably in the dorsal and medial lobes (Fig. S5C). The frequency of segregation defects in *Dscam1*$^{\Delta 9uD}$ mutants was not significantly lower than that of *Dscam1*^{null} mutants (Fig. S5C). However, we also seldom observed fascicles or crossings between sister branches in *Dscam1*$^{\Delta 9uD}$ neurons (Fig. S5B), whereas axonal sister branches in *Dscam1*^{null} neurons were extensively crossed (6, 7, 9, 17, 22). These data indicate that altered composition of Dscam1 isoforms does not affect the repulsion of self-branches from the same neuron. Thus, the phenotypic defects observed in *Dscam1*$^{\Delta 9uD}$ mutants should not be attributed to the absence of self-repulsion between sister branches of the same neuron. Given the considerable changes in the expression pattern of MB single neurons between WT and *Dscam1*$^{\Delta 9uD2–\Delta 9uD5}$ mutant (Fig. 2B), we speculate that Dscam1 isoforms are intrinsically required for MB development.

Altered composition of Ig7 variants causes mild axonal defects in MS neurons

Axons of adult *Drosophila* scutellar MS neurons project to the ventral nerve cord and form stereotyped branches to connect with

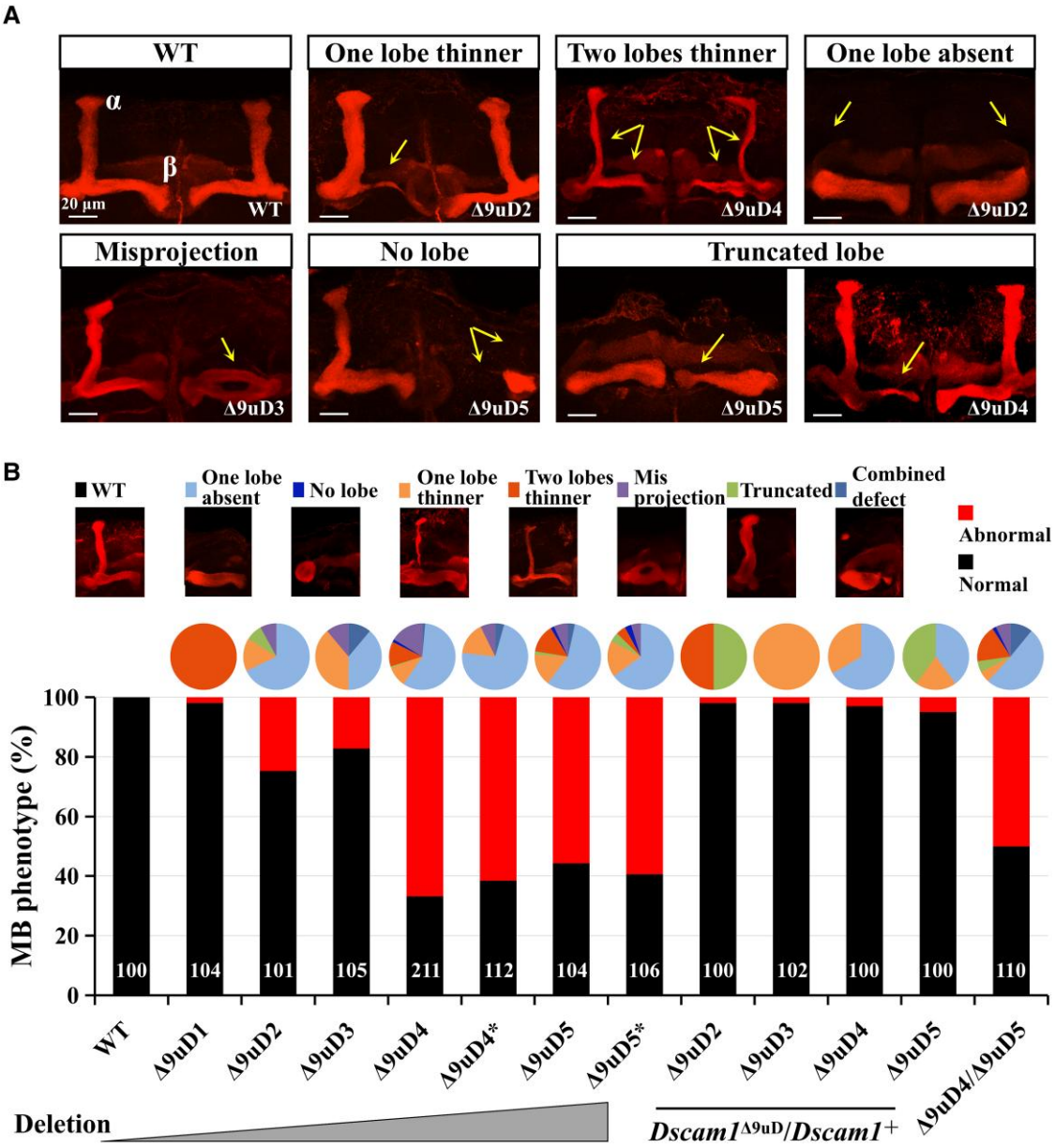

Fig. 4. Altered composition of Ig7 variants resulting in MB defects (see also Fig. S4). A) Representative images of MB lobe defects in mutant animals. Anti-FasII staining visualizes the α- and β-lobes of mushroom bodies in the adult brain. Arrows indicate lobe defects. Scale bars, 20 μm. B) MB phenotypes of *Dscam1*$^{\Delta 9uD}$ mutant flies. The pie charts above the bar graph display the proportion of different types of MB defects in different mutants, respectively. Numbers in parentheses represent the numbers of brain hemispheres examined for each genotype. *Dscam1*$^{\Delta 9uD4*}$ and *Dscam1*$^{\Delta 9uD5*}$, which lacked the same sequence as *Dscam1*$^{\Delta 9uD4}$ and *Dscam1*$^{\Delta 9uD5}$, were generated independently via homologous recombination.

multiple postsynaptic partners in different territories. Many features of the axonal branching pattern of MS neurons are genetically hardwired, such as the position of primary or secondary axonal branches, the direction of branch extension, and the length of branch extension (Fig. 6A). In sharp contrast to its canonical role in self and nonself-recognition in da neurons and MB neurons, Dscam1 diversity serves as a cell-intrinsic regulator of Dscam1 signaling strength to control the formation of axon branch collateral in MS neurons (10). To further investigate the role of Dscam1 isoform composition in neuronal wiring, we examined the axonal branching pattern of MS neurons. We found that MS neurons of *Dscam1*$^{\Delta 9uD1-\Delta 9uD5}$ showed subtle to mild defects in their characteristic overall shape and axonal branching patterns of posterior scutellar neurons compared with WT controls (Figs. 6B and C and S6A). The primary ipsilateral axon shaft was consistently formed, but some collateral branches were truncated or even missing, which varied in different *Dscam1*$^{\Delta 9uD}$ mutants (Figs. 6B and C and S6A). For example, ~15% of *Dscam1*$^{\Delta 9uD2}$ and *Dscam1*$^{\Delta 9uD5}$ MS neurons completely or partially lost their lateroanterior branches (branch 2), whereas 100% of WT control had these branches. Further statistical analyses revealed a significant decrease in the length of branch 2 in *Dscam1*$^{\Delta 9uD2}$ compared with the WT control (Fig. 6D). These data indicate that these differences in the same position persist across the same mutants and different genetic backgrounds (Figs. 6D and S6). Since identical branching defects were observed in mutants with deletion of docking sites in the exon 6 cluster with altered composition of the Ig3 variant (33), we conclude that the branching defects seen in *Dscam1*$^{\Delta 9uD}$ mutants mainly originate from the altered composition of the Dscam1 Ig7 variants.

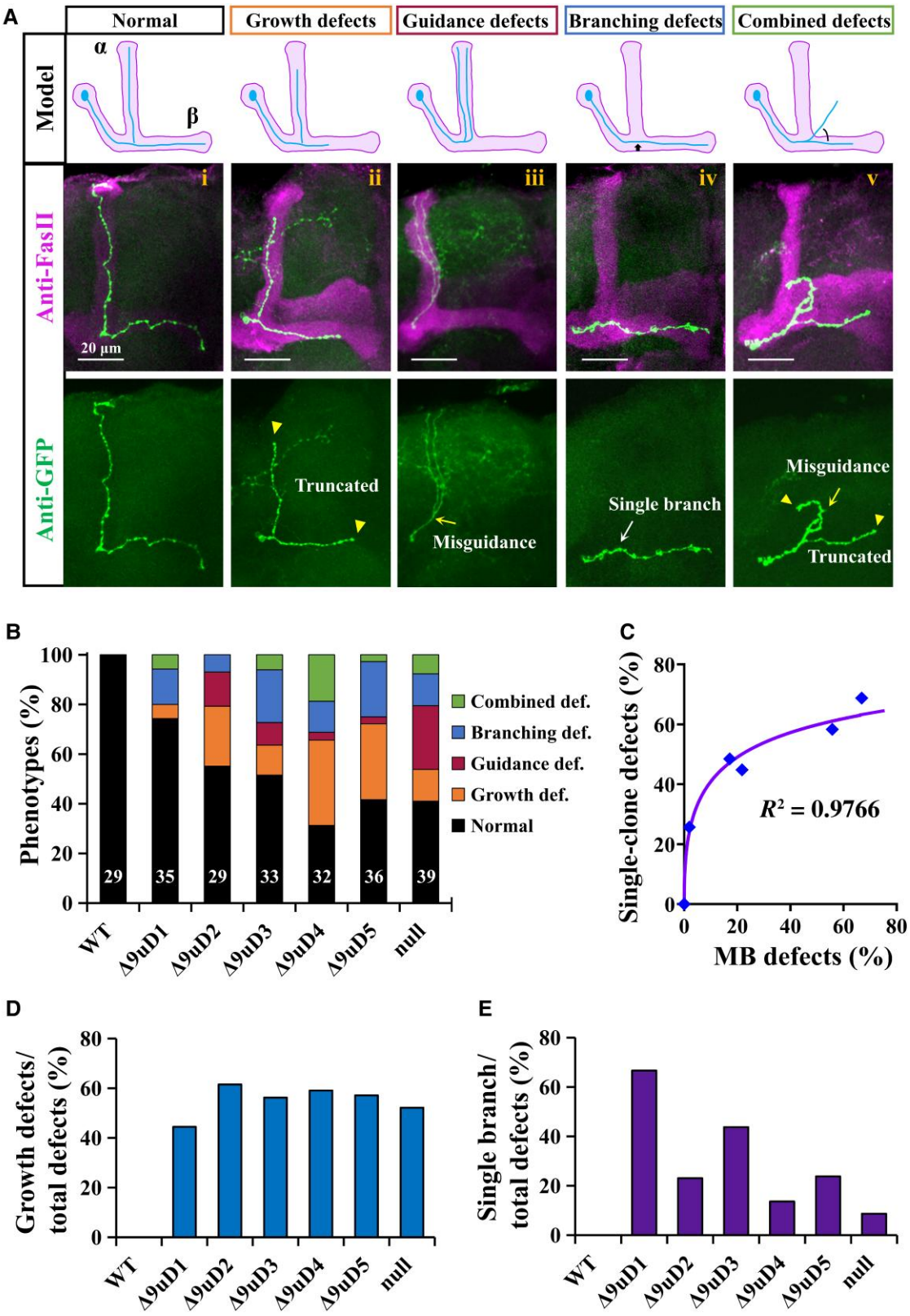

Fig. 5. Phenotypic analysis of *Dscam1*$^{\Delta 9uD}$ mutant MB axons in single-cell clones (see also Fig. S5). A) Common types of monoclonal development defects in mushroom bodies. All schematic drawings are illustrated for the adult MB of the brain hemispheres. (Top) Models of different defects. (Middle and bottom) Representative images of single-cell clone defects. Anti-FasII staining visualizes the whole mushroom bodies (magenta), while single-cell clones show green (anti-GFP). (Middle) i, WT; ii, growth defect; iii, guidance defect; iv, single branch; v, combined defect showing both growth and guidance defect. (Bottom) Scale bars, 20 μm. B) Quantification of MB axon defects in single-cell clones. Numbers in parentheses denote single clones analyzed for each mutant. C) Whole MB defects being strongly correlated with single-clone defects. D) *Dscam1*$^{\Delta 9uD1-\Delta 9uD5}$ showing a high proportion of axonal growth defects. E) *Dscam1*$^{\Delta 9uD1-\Delta 9uD5}$ showing a high proportion of single axonal branches.

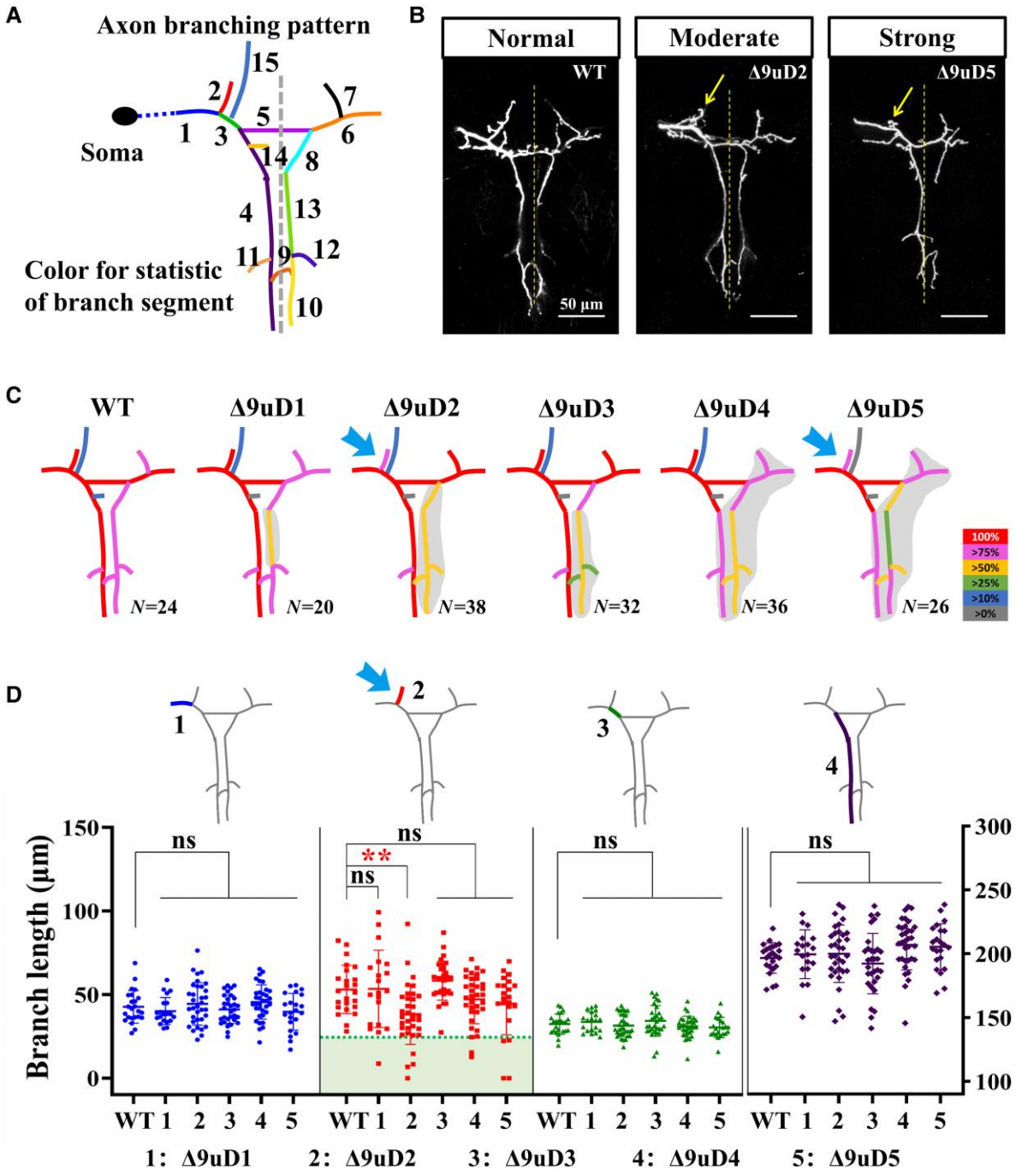

Fig. 6. Altered composition of Ig7 variants resulting in subtle axonal defects in MS neurons (see also Fig. S6). A) Schematic representation of the axon trajectory of a single MS neuron within the CNS. Different colors represent the statistical length and frequency of a segment. Branching and sectioning refer to previous study (8). B) Branching patterns of MS neurons in control and mutant animals. Arrows indicate missing or shorter lateroanterior branches. The dashed line indicates the midline of the CNS. Scale bars, 50 μm. C) Frequency of each segment of MS neuron in WT and *Dscam1*$^{\Delta 9uD1-\Delta 9uD5}$ is shown. The letter *N* in the right subscript represents the number of analyzed neurons. Different colors represent different frequencies of the segments. D) Quantification of the length of segments 1 to 4 of MS neurons in *Dscam1*$^{\Delta 9uD1-\Delta 9uD5}$. The corresponding statistical segment is shown on each cluster scatter plot. The missing branch length is denoted as 0. Data are expressed as mean ± SD. *, $P < 0.05$; **, $P < 0.01$; ns, not significant (Student's *t*-test, two-tailed). Quantification of the length of segments 5 to 8 of MS neurons in *Dscam1*$^{\Delta 9uD1-\Delta 9uD5}$ was shown in Fig. S6B.

Opposite effects of lowering Dscam1 levels on dendritic and axonal defects caused by altered composition of Ig7 variants

To further elucidate the molecular mechanisms underlying the observed developmental defects, we examined the effect of reducing Dscam1 levels on the phenotypes of *Dscam1*$^{\Delta 9uD1-\Delta 9uD5}$ flies. We compared *Dscam1*$^{\Delta 9uD}$/*Dscam1*^{null} flies, where the overall expression level of Dscam1 was reduced by ~50% relative to *Dscam1*$^{\Delta 9uD}$ and WT controls (Fig. S7A). We found that the survival rate of *Dscam1*$^{\Delta 9uD1-\Delta 9uD5}$/*Dscam1*^{null} flies was restored up to ~90% compared with 70–85% for *Dscam1*$^{\Delta 9uD1-\Delta 9uD5}$ homozygous flies (Figs. 7A, panel i and S7B). In contrast, reducing Dscam1 levels in *Dscam1*$^{\Delta 9uD1-\Delta 9uD5}$ mutants aggravated climbing ability defects in larvae and adults compared with *Dscam1*$^{\Delta 9uD1-\Delta 9uD5}$ homozygous

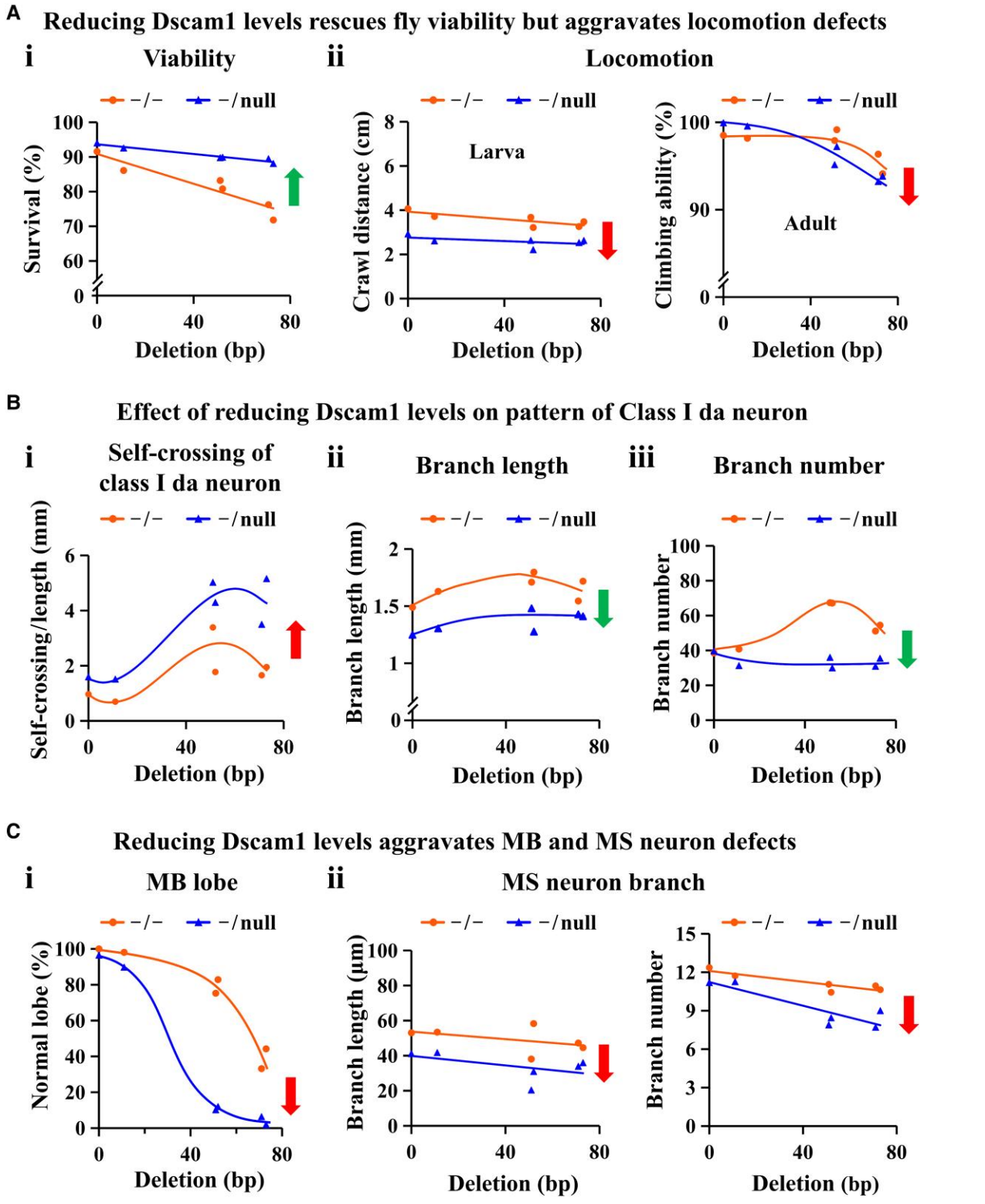

Fig. 7. Effect of reducing Dscam1 expression levels on the phenotypic defects changing with the deleted sequence (see also Figs. S7–S10). A) Reducing Dscam1 expression rescues fly viability (panel i) but aggravates locomotion defects (panel ii). And the longer the deleted sequence, the more obvious complement or aggravation phenotype in $Dscam1^{\Delta 9uD}/Dscam1^{null}$. B) Reducing Dscam1 levels shows increased self-crossing (panel i) but reduced branch and length (panel ii) in class I da neuron. C) Reducing Dscam1 expression levels aggravates MB (panel i) and MS (panel ii) neuron defects. The direction of the arrow indicates the direction of phenotypic change following reduced protein expression, and the color of the arrow indicates the reversion (green) or aggravation (red) of the phenotype relative to the WT.

flies (Figs. 7A, panel ii and S7C). Taken together, these data indicate that reducing Dscam1 levels differentially affects fly viability and locomotion defects caused by the altered Ig7 composition.

Analysis of $Dscam1^{\Delta 9uD}/Dscam1^{null}$ mutant flies showed that removing one copy of the mutant *Dscam1* led to significant reductions in total dendritic length and number compared with

homozygous mutants with two copies of *Dscam1*$^{\Delta 9uD}$, thereby reverting these defects to the WT level (Figs. 7B, panels ii and iii and Fig. S8A). These data suggest that a reduction in the Dscam1 protein level can rescue the growth and branching defects caused by the altered composition of exon 9 variants. However, we found significant increases in the number of crossing between self-dendrites in class I da neurons compared with homozygous mutants carrying two copies of *Dscam1*$^{\Delta 9uD}$ ($P < 0.05$) (Figs. 7B, panel i and S8B, panel i). We speculate that significant increases in self-crossing following the removal of one copy of the *Dscam1* gene may be due to a decrease in overall homophilic binding strength. Thus, reducing Dscam1 levels in *Dscam1*$^{\Delta 9uD}$ has two contrasting effects on dendritic patterning: aggravating self-avoidance defects but alleviating growth and branching defects. The opposite effects of lowering Dscam1 dosage on dendrite patterning also suggest a dual role for Dscam1 isoforms in dendritic patterning.

Next, we examined the MB phenotypes of *Dscam1*$^{\Delta 9uD}$/*Dscam1*^{null} mutants. Unexpectedly, removal of one copy of the mutant *Dscam1* resulted in a remarkable increase in MB defects in all *Dscam1*$^{\Delta 9uD1–\Delta 9uD5}$ mutants. Notably, *Dscam1*$^{\Delta 9uD2}$/*Dscam1*^{null} and *Dscam1*$^{\Delta 9uD3}$/*Dscam1*^{null} exhibit MB defects in up to 90% of brain hemispheres, compared with ∼20% of defects in the homozygous mutants with two copies of *Dscam1*$^{\Delta 9uD2}$ and *Dscam1*$^{\Delta 9uD3}$. Similarly, removing one copy of the mutant *Dscam1* resulted in a substantial increase from 56 to 98% of MB defects in *Dscam1*$^{\Delta 9uD5}$ mutants (Figs. 7C, panel i and S8B, panel ii). These data suggest that the MB morphology shows strikingly different sensitivities to disruption of exon 9 compositions at different levels of Dscam1 protein.

We also noted that removal of one copy of the mutant *Dscam1* resulted in a striking increase in MS axonal branching defects in *Dscam1*$^{\Delta 9uD}$ mutants (Fig. 7C, panel ii). For example, the length of branch 2 in *Dscam1*$^{\Delta 9uD2}$/*Dscam1*^{null} was reduced to 20 μm compared with 38 μm in homozygous mutants carrying two copies of *Dscam1*$^{\Delta 9uD2}$ (Fig. S8C, panel ii). Likewise, we observed a significant reduction in the length of some other branches in *Dscam1*$^{\Delta 9uD2–\Delta 9uD5}$/*Dscam1*^{null} compared to *Dscam1*$^{\Delta 9uD2–\Delta 9uD5}$ (Fig. S8C, panel iii). The reduction in branch length persists in mutants of different genetic backgrounds or in *Dscam1*$^{\Delta 9uD1–\Delta 9uD5}$/*Dscam1*^{null} *trans*-heterozygous mutants (Fig. 7C, panel ii). These data also suggest that normal branching of posterior scutellar neurons requires not only the number of Dscam1 isoforms but also the overall expression level or their specific composition (at least for Ig7).

In summary, reducing Dscam1 levels remarkably affects developmental defects caused by the altered composition of Ig 7 variants, but the magnitude and direction of the effect vary based on individual phenotype and mutant. Removing one copy of the mutant *Dscam1* improves fly viability but aggravates the locomotor defects caused by altered isoform composition. Similarly, reducing Dscam1 levels restores normal growth of da mutant neurons but leads to more severe axon and dendrite patterning defects in MB and MS neuronal defects caused by altered isoform composition (Figs. 7, S7, and S8). However, the effects on a particular phenotype were identical among the different mutants, positing a functional link between Dscam1 expression levels and isoform composition. These results also suggest that Dscam1 isoforms mediate different developmental contexts and neuronal wiring via distinct mechanisms.

Discussion

Our present study reveals extensive noncanonical functions of Dscam1 isoforms in neuronal wiring. Rather than deleting the coding exon region as in other previous studies, we deleted the noncoding *cis*-elements using CRISPR/Cas9. Surprisingly, this led to the creation of a genetic system appropriate for studying the importance of Dscam1 isoform composition. These resulting Dscam1 isoform composition-altered mutants exhibited normal dendritic self-avoidance and self-/nonself-discrimination in da neurons, which is consistent with the canonical self-avoidance model. Surprisingly, these mutants exhibited strikingly distinct spectra of phenotypic defects in three types of neurons: up to ∼60% defects in mushroom bodies, significantly increased branching and growth in da neurons, and mild axonal branching defects in MS neurons. These data suggest that the Dscam1 isoform composition is cell-autonomously required for normal neurite growth of diverse neurons. Moreover, this splicing-tuned genetic strategy provides insights into the biological functions of Dscam1 isoforms.

Dscam1 isoform composition is cell-autonomously required for normal dendrite branching and growth of da neurons

Numerous studies have shown that Dscam1 functions to mediate dendrite patterning via homophilic repulsion in da neurons (8, 19, 22, 24, 26, 27, 34). However, our present study shows that altered Dscam1 isoform composition leads to significant increases in the number of dendritic branches and total dendritic length without disrupting dendritic spacing or interneuronal repulsion. No obvious dendritic self-crossings were observed, and the overlap between class I (vpda) and class III (v′pda) dendrites was not affected. Thus, in addition to its canonical role in dendrite self-avoidance, this study reveals a previously unrecognized function of Dscam1 in *Drosophila* PNS development; that is, Dscam1 autonomously regulates dendrite branching and growth. This idea is also supported by the contrasting effect on dendritic patterning by reducing Dscam1 levels: increasing self-avoidance errors but alleviating growth defects (Figs. 7 and S9). Similarly, a previous study using RNAi knockdown has demonstrated that Dscam1 is required for normal dendrite growth and branching, but not for dendritic spacing and intraneuronal repulsion in fly motoneurons (14), which indicates that self-repulsion in motoneurons may be mediated by other molecules or mechanisms. Collectively, these data suggest that Dscam1 isoforms play a conserved role in dendritic arbor growth and branching of both central and peripheral neurons.

How does Dscam1 isoforms affect dendritic branch formation? Our present study suggests that Dscam1 isoforms may mediate dendritic branch formation via a mechanism distinct from self-avoidance. In the canonical model of self-avoidance, specific isoforms are not required; what is important is that each neuron has a Dscam1 repertoire distinct from that of its neighbors (8). However, our data indicate that the specific Dscam1 repertoire of each cell may affect the length and number of dendrite branches. Thus, a specific Dscam1 repertoire for each neuron is cell-intrinsically required for normal dendrite growth and branching. Previous studies showed that loss of Dscam1 function does not obviously affect the length and the number of da dendrite branches (24, 34), which led us to wonder whether the branching and growth phenotypic defects in *Dscam1*$^{\Delta 9uD2–\Delta 9uD5}$ mutants are caused by gain-of-function signaling. Moreover, our data show that reducing Dscam1 levels in *Dscam1*$^{\Delta 9uD}$ enhances dendritic self-repulsion but restores normal dendritic growth and branching (Fig. 7B), which suggest that Dscam1 mediates self-avoidance and branch formation via different signaling pathways. It is understandable that removing one copy of the mutant *Dscam1*

reduced homophilic interaction strength and then increased self-crossing, which is compatible with the canonical self-avoidance model (3, 7, 8, 19, 24, 34). By contrast, removing one copy of the mutant *Dscam1* might decrease the gain-of-function effect caused by the altered isoform composition and then alleviate growth and branching defects. Since dendritic self-avoidance in da neurons does not require PAK1 (24) and *Dscam1*$^{\Delta 9uD2}$ mutants are partially similar to PAK overexpression mutants that exhibit excessive branching in ddaE neurons, we speculate that PAK may be a candidate for regulating Dscam1-mediated dendritic branching and growth. Further biochemical and genetic studies will be required to elucidate the mechanism of Dscam1 isoforms in dendritic branch formation.

Extensive noncanonical functions of Dscam1 isoforms in neuronal wiring

The canonical model of Dscam1-mediated self-avoidance has been illustrated in MB axonal segregation (7, 8, 11, 12, 35). Self-branches are mutually recognized via homophilic interactions of the Dscam1 isoform, which trigger repulsion signaling and subsequent segregation of high-fidelity axonal branches. However, this model cannot account for several findings in our present study. First, the *Dscam1*$^{\Delta 9uD4}$ allele, which potentially generates a comparable isoform number to the WT control, exhibited normal dendritic self-avoidance and self-/nonself-discrimination but displayed more than 67% defects in mushroom bodies. In particular, removing one copy of the mutant *Dscam1* leads to nearly 100% MB defects in the *Dscam1*$^{\Delta 9uD4}$/*Dscam1*^{null} and *Dscam1*$^{\Delta 9uD5}$/*Dscam1*^{null} mutants (Figs. 7C, panel i and S8B, panel ii). Thus, the high penetrance of MB phenotypes caused by altered isoform composition cannot be fully explained by the Dscam1-mediated self-avoidance model.

Second, our mosaic analysis of single mutant neurons with altered Dscam1 isoform composition revealed ~70% of axonal defects, of which 70~90% fell into the category of growth and branching defects. Notably, 44% of *Dscam1*$^{\Delta 9uD3}$ neurons exhibited only a single branch (Fig. 5E). These data demonstrate that the appropriate composition of Dscam1 isoforms is required for normal bifurcation of MB axons. Furthermore, the shortened axon phenotype caused by altered isoform composition obviously could not be fully explained by Dscam1-mediated self-avoidance. In addition, the altered Dscam1 isoform composition caused a high frequency of abnormal branch segregation. Taken together, our data suggest that axonal wiring is largely mediated via a mechanism distinct from canonical self-avoidance.

However, it remains unclear how Dscam1 isoform composition affects axonal wiring. We considered several possible scenarios. First, alterations in Ig7 variant composition affect signaling strength mediated by Dscam1 homophilic binding, which in turn modulates axon growth and branching, as previously proposed in posterior scutellar MS neurons (10). However, this hypothesis appears to be inconsistent with our observation that removal of one copy of the mutant *Dscam1* exacerbates MB defects caused by the altered isoform composition. Thus, these MB defects in *Dscam1*$^{\Delta 9uD}$ mutants should not be attributed primarily to overactivation of Dscam1 signaling due to the increased homophilic binding strength. Conversely, it seems plausible that the altered isoform composition may lead to underactivation of Dscam1 signaling and that lowering Dscam1 levels exacerbates these defects, but this is currently speculation. The second possible mechanism is that Dscam1 isoforms affect the ligand–receptor interactions that regulate axonal growth cone dynamics. Several studies have shown that Dscam1 is able to bind to a few well-characterized secreted ligands involved in neuronal wiring. For example, netrin binds to both fly and vertebrate Dscam1 via the Ig7 domain (36–38), while Dscam1 binds Slit-N via at least two binding sites in the first five Ig domains, one of which lies in the first three Ig domains (39). Slit binding and subsequent increased Dscam1 dephosphorylation by RPTP69D modulated Dscam1 signaling to locally control axon branch growth in circuit formation (40). This variable domain specificity is also supported by evidence that a cluster-specific deletion of the docking site in the exon 4 cluster results in only a subtle MB defect (<4%) (27), whereas a deletion of the docking site in the exon 6 cluster results in ~5% MB defect (33). In contrast, our present study shows that altered composition of Ig7 variants causes as high as 60% of MB defects. These data indicate that Dscam1 isoforms mediate MB axonal patterning in a variable domain-specific manner. Alternatively, altering Ig7 variant composition may affect adhesive interactions between axon branches from different neurons (12, 22, 41, 42). All in all, Dscam1 isoforms may play multifaceted roles in neuronal wiring via combinatorial mechanisms.

Our present study also shows that Dscam1 isoforms play a differential role in the growth and development of dendrites and axons in different neurons. Interestingly, global alterations in exon 9 variant composition increased dendritic growth and branches in da neurons but inhibited MB and MS axonal branching and growth. These contrasting effects were influenced by overall Dscam1 levels: reducing the levels of Dscam1 restores normal dendritic growth in da neurons but aggravates MS axonal growth. These results further support the notion that Dscam1 isoforms mediate dendritic and axonal growth via distinct pathways. In summary, these present results, together with previous studies (10, 26), suggest extensive noncanonical functions of Dscam1 isoforms in neuronal wiring.

Are the specific (subsets of) Dscam1 isoforms important?

Previous genetic studies have suggested that the specificity of individual Dscam1 isoforms may not be functionally important (6–10, 13). However, these functional experiments using overexpression of a single isoform, knock-ins, or genomic deletions caused defective phenotypes that were either too strong or too weak to unmask functional differences between individual isoforms. Alternatively, loss-of-function phenotypic differences between them could easily be overridden by gain of function. In the present study, we employed CRISPR/Cas9 technique to delete the intronic regulatory sequences, which allowed us to assess the importance of the compositional specificity of Ig7 variants. We reasoned that if the individual Ig7 variants are functionally identical, the altered composition of the exon 9 variants should not cause obvious phenotypic defects. Indeed, these mutants exhibit normal dendritic self-avoidance and self-/nonself-discrimination in da neurons. However, all global alterations in the composition of exon 9 variants result in abnormal growth and development of all three types of neurons (Fig. S9). Moreover, there was a differential dependence with the largest effect on increased da dendritic branching in *Dscam1*$^{\Delta 9uD2}$, MB defects in *Dscam1*$^{\Delta 9uD4}$, and MS neurons in *Dscam1*$^{\Delta 9uD2}$ (Fig. S9). Collectively, we provide clear evidence supporting the differential role of Dscam1 Ig7 subsets (if not individual Ig7 variants) in the regulation of neuronal growth and branching.

Dscam1 level, diversity, and composition

Previous studies have shown that the *Dscam1* gene mediates fly development by tuning overall isoform levels, diversity, and

composition (6–10, 13, 14, 17–24, 26, 27, 34, 43–45). However, the functional link between them remains unclear. Our current study shows that reducing Dscam1 levels has distinct effects on the different developmental defects caused by altered isoform composition (Fig. S9). These results suggest that Dscam1 isoforms mediate different developmental contexts through distinct mechanisms. Interestingly, this is inconsistent with our observation that reducing the expression levels of Dscam1 remarkably decreases the behavioral and neuronal defects caused by reduced Dscam1 diversity (Figs. S9 and S10A and B) (26). Thus, our data reveal a distinct effect of lowering Dscam1 levels on phenotypes between isoform diversity and composition (Fig. S9). Lowering Dscam1 levels exacerbates MB and MS neuronal defects caused by disruption of isoform composition, but it reduces MB and MS neuronal defects caused by reduced isoform diversity. Similar trends in locomotion have been observed. Cross-correlation analyses of different phenotypes also revealed considerably different correlations when removing one copy of the mutant *Dscam1* (Fig. S10C). These data suggest that Dscam1 isoform composition may function via a mechanism distinct from isoform diversity. However, lowering Dscam1 levels revert the viability and class I da neuronal branching caused by reduced isoform diversity and altered isoform composition (Figs. S7B, S8A, and S10A and B). Thus, our study reveals a shared and distinct effect of lowering Dscam1 levels on phenotypes between Dscam1 isoform diversity and composition. These findings also point to a complex functional link between Dscam1 expression levels, isoform diversity, and composition.

Materials and methods

Generation of fly *Dscam1* mutant alleles

We used the CRISPR/Cas9 system to delete or mutate the docking site in the *Drosophila Dscam1* gene (details are in Supplementary Methods). The primers and sgRNAs can be found in Table S1.

Detection of Dscam1 isoform expression at a single-neuron resolution

Single cells were obtained by dissociation through trypsin-EDTA (0.05%, Invitrogen_25300054) or collagenase I (100 mg/mL, Invitrogen_17100-017). Then, GFP+ single cells were obtained by flow cytometer sorter (Beckman Coulter MoFlo XDP). Single-cell lysis and reverse transcription methods were referenced to the SMART-seq2 method (31). Finally, we calculated the relative expression levels of *Dscam1* exon 9s according to the method as previously described (27) (details are in Supplementary Methods).

Immunostaining

Third instar larvae on the tube wall were used to detect the growth, branching, and coexistence of da neurons. Dissection was performed in a silicone-coated dish containing phosphate-buffered saline (PBS) and stretched and fixed with 4% paraformaldehyde at room temperature for 25 min. HRP antibody (Cy3-conjugated AffiniPure Goat Anti-Horseradish Peroxidase, diluted 1:200) was used to stain all da neurons. Adult head dissection was also performed in cold PBS and fixed in 4% paraformaldehyde for 45 min at room temperature. Primary antibodies (anti-FasII, DSHB, diluted 1:2 in PBST) and secondary antibodies (Alexa594-goat-anti-mouse IgG, EarthOx, diluted 1:400 in PBST) were used for immunofluorescence staining. Finally, da neurons and mushroom bodies were imaged with a laser scanning confocal microscope LSM800 (Carl Zeiss) (details are in Supplementary Methods).

Supplementary material

Supplementary material is available at *PNAS Nexus* online.

Funding

This work was supported by research grants from the National Key Research and Development Program of China (2021YFE0114900), the National Natural Science Foundation of China (91940303 and 91740104 to Y.J.; 31671510 and 31871461 to H.H.), the Natural Science Foundation of Zhejiang Province (LD21C050002), and the Starry Night Science Fund at Shanghai Institute for Advanced Study of Zhejiang University (SN-ZJU-SIAS-009). This manuscript was posted on a preprint [doi: https://doi.org/10.1101/2022.04.14.488281].

Author contributions

Y.J. conceived of this project. S.Z., X.Y., H.D., J.Z., and L.W. designed and performed the experiments. S.Z., L.W., B.X., H.D., P.G., Y.Z., and J.Z. participated in the construction and screening of the mutants. S.Z., X.Y., L.L., Y.F., and Y.D. performed the phenotype analysis. S.Z., P.G., G.L., J.S., and F.S. analyzed the data. Y.J., H.H., J.H., S.Z., and G.L. wrote the manuscript. All authors discussed the results and commented on the manuscript.

Data availability

All other data and details about materials and methods used are present in the article and supplementary material.

References

1 Schmucker D, *et al.* 2000. Drosophila Dscam is an axon guidance receptor exhibiting extraordinary molecular diversity. *Cell* 101: 671–684.
2 Wu Q, Maniatis T. 1999. A striking organization of a large family of human neural cadherin-like cell adhesion genes. *Cell* 97: 779–790.
3 Wojtowicz WM, *et al.* 2007. A vast repertoire of Dscam binding specificities arises from modular interactions of variable Ig domains. *Cell* 130:1134–1145.
4 Neves G, Zucker J, Daly M, Chess A. 2004. Stochastic yet biased expression of multiple Dscam splice variants by individual cells. *Nat Genet.* 36:240–246.
5 Miura SK, Martins A, Zhang KX, Graveley BR, Zipursky SL. 2013. Probabilistic splicing of Dscam1 establishes identity at the level of single neurons. *Cell* 155:1166–1177.
6 Zhan XL, *et al.* 2004. Analysis of Dscam diversity in regulating axon guidance in Drosophila mushroom bodies. *Neuron* 43: 673–686.
7 Hattori D, *et al.* 2007. Dscam diversity is essential for neuronal wiring and self-recognition. *Nature* 449:223–227.
8 Hattori D, *et al.* 2009. Robust discrimination between self and non-self neurites requires thousands of Dscam1 isoforms. *Nature* 461:644–648.
9 Wang J, *et al.* 2004. Transmembrane/juxtamembrane domain-dependent Dscam distribution and function during mushroom body neuronal morphogenesis. *Neuron* 43:663–672.
10 He HH, *et al.* 2014. Cell-intrinsic requirement of Dscam1 isoform diversity for axon collateral formation. *Science* 344:1182–1186.
11 Zipursky SL, Sanes JR. 2010. Chemoaffinity revisited: dscams, protocadherins, and neural circuit assembly. *Cell* 143:343–353.

12 Sanes JR, Zipursky SL. 2020. Synaptic specificity, recognition molecules, and assembly of neural circuits. *Cell* 181:536–556.
13 Kim JH, Wang X, Coolon R, Ye B. 2013. Dscam expression levels determine presynaptic arbor sizes in Drosophila sensory neurons. *Neuron* 78:827–838.
14 Hutchinson KM, Vonhoff F, Duch C. 2014. Dscam1 is required for normal dendrite growth and branching but not for dendritic spacing in Drosophila motoneurons. *J Neurosci*. 34:1924–1931.
15 Wilhelm N, Kumari S, Krick N, Rickert C, Duch C. 2022. Dscam1 has diverse neuron type-specific functions in the developing Drosophila CNS. *eNeuro* 9:ENEURO.0255-22.2022.
16 Liu C, *et al*. 2020. Dscam1 establishes the columnar units through lineage-dependent repulsion between sister neurons in the fly brain. *Nat Commun*. 11:4067.
17 Wang J, Zugates CT, Liang IH, Lee CHJ, Lee T. 2002. Drosophila Dscam is required for divergent segregation of sister branches and suppresses ectopic bifurcation of axons. *Neuron* 33:559–571.
18 Zhu H, *et al*. 2006. Dendritic patterning by Dscam and synaptic partner matching in the Drosophila antennal lobe. *Nat Neurosci*. 9:349–355.
19 Soba P, *et al*. 2007. Drosophila Sensory neurons require Dscam for dendritic self-avoidance and proper dendritic field organization. *Neuron* 54:403–416.
20 Shi L, Yu HH, Yang JS, Lee T. 2007. Specific Drosophila Dscam juxtamembrane variants control dendritic elaboration and axonal arborization. *J Neurosci*. 27:6723–6728.
21 Chen BE, *et al*. 2006. The molecular diversity of Dscam is functionally required for neuronal wiring specificity in Drosophila. *Cell* 125:607–620.
22 Wu W, Ahlsen G, Baker D, Shapiro L, Zipursky SL. 2012. Complementary chimeric isoforms reveal Dscam1 binding specificity in vivo. *Neuron* 74:261–268.
23 Cvetkovska V, Hibbert AD, Emran F, Chen BE. 2013. Overexpression of Down syndrome cell adhesion molecule impairs precise synaptic targeting. *Nat Neurosci*. 16:677–682.
24 Hughes ME, *et al*. 2007. Homophilic Dscam interactions control complex dendrite morphogenesis. *Neuron* 53:417–427.
25 Yu HH, Yang JS, Wang J, Huang Y, Lee T. 2009. Endodomain diversity in the Drosophila Dscam and its roles in neuronal morphogenesis. *J Neurosci*. 29:1904–1914.
26 Dong H, *et al*. 2022. Self-avoidance alone does not explain the function of Dscam1 in mushroom body axonal wiring. *Curr Biol*. 32:2908–2920.e4.
27 Hong W, *et al*. 2021. Intron-targeted mutagenesis reveals roles for Dscam1 RNA pairing architecture-driven splicing bias in neuronal wiring. *Cell Rep*. 36:109373.
28 Yang Y, *et al*. 2011. RNA Secondary structure in mutually exclusive splicing. *Nat Struct Mol Biol*. 18:159–168.
29 Yue Y, *et al*. 2016. Long-range RNA pairings contribute to mutually exclusive splicing. *RNA* 22:96–110.
30 Dong H, *et al*. 2021. Complex RNA secondary structures mediate mutually exclusive splicing of Coleoptera *Dscam1*. *Front Genet*. 12:644238.
31 Picelli S, *et al*. 2014. Full-length RNA-seq from single cells using Smart-seq2. *Nat Protoc*. 9:171–181.
32 Lee T, Luo L. 1999. Mosaic analysis with a repressible cell marker for studies of gene function in neuronal morphogenesis. *Neuron* 22:451–461.
33 Dong H, Xu B, Guo P, Zhang J, Yang X. 2022. Hidden RNA pairings counteract the "first-come, first-served" splicing principle to drive stochastic choice in Dscam1 splice variants. *Sci Adv*. 8:eabm1763.
34 Matthews BJ, *et al*. 2007. Dendrite self-avoidance is controlled by Dscam. *Cell* 129:593–604.
35 Hattori D, Millard SS, Wojtowicz WM, Zipursky SL. 2008. Dscam-mediated cell recognition regulates neural circuit formation. *Annu Rev Cell Dev Biol*. 24:597–620.
36 Andrews GL, *et al*. 2008. Dscam guides embryonic axons by netrin-dependent and -independent functions. *Development* 135:3839–3848.
37 Liu GF, *et al*. 2009. DSCAM Functions as a netrin receptor in commissural axon pathfinding. *P Natl Acad Sci U S A*. 106:2951–2956.
38 Ly A, *et al*. 2008. DSCAM Is a netrin receptor that collaborates with DCC in mediating turning responses to netrin. *Cell* 133:1241–1254.
39 Alavi M, *et al*. 2016. Dscam1 forms a Complex with robo1 and the N-terminal fragment of slit to promote the growth of longitudinal axons. *PLoS Biol*. 14:e1002560.
40 Dascenco D, *et al*. 2015. Slit and receptor tyrosine phosphatase 69D confer spatial specificity to axon branching via Dscam1. *Cell* 162:1140–1154.
41 Schmucker D, Chen B. 2009. Dscam and DSCAM: complex genes in simple animals, complex animals yet simple genes. *Genes Dev*. 23:147–156.
42 Shi L, Lee T. 2012. Molecular diversity of dscam and self-recognition. *Adv Exp Med Biol*. 739:262–275.
43 Lowe SA, Hodge JJL, Usowicz MM. 2018. A third copy of the Down syndrome cell adhesion molecule (Dscam) causes synaptic and locomotor dysfunction in Drosophila. *Neurobiol Dis*. 110:93–101.
44 Sterne GR, Kim JH, Ye B. 2015. Dysregulated Dscam levels act through Abelson tyrosine kinase to enlarge presynaptic arbors. *eLife* 4:e05196.
45 Hummel T, *et al*. 2003. Axonal targeting of olfactory receptor neurons in Drosophila is controlled by Dscam. *Neuron* 37:221–231.
46 Palavalli A, Tizon-Escamilla N, Rupprecht JF, Lecuit T. 2021. Deterministic and stochastic rules of branching govern dendrite morphogenesis of sensory neurons. *Curr Biol*. 31:459–472.e454.